A novel lumped thermal characteristic modeling strategy for the online adaptive temperature and parameter co-estimation of vehicle lithium-ion batteries.
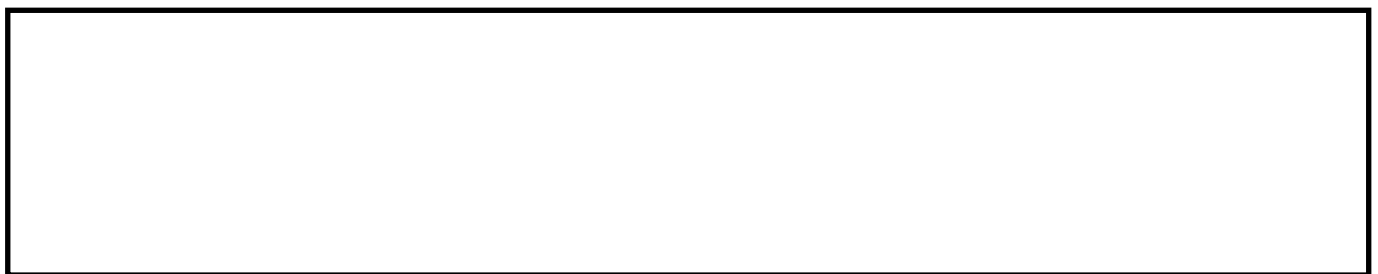
SHI, H., WANG, L., WANG, S., FERNANDEZ, C., XIONG, X., DABLU, B.E. and XU, W.

2022

A novel lumped thermal characteristic modeling strategy

for the online adaptive temperature and parameter co-estimation

of vehicle lithium-ion batteries

Haotian Shi[a], Liping Wang[a,b], Shunli Wang[a*], Carlos Fernandez[c], Xin Xiong[a,d], Bobobee Etse Dablu[a], Wenhua Xu[a]

[a]School of Information Engineering, Southwest University of Science and Technology, Mianyang 621010, China;

[b]State Key Laboratory of Tribology and Institute of Manufacturing Engineering, Department of Mechanical Engineering, Tsinghua University, Beijing 100084, China;

[c]School of Pharmacy and Life Sciences, Robert Gordon University, Aberdeen AB10-7GJ, UK;

[d]Department of Automation, University of Science and Technology of China, Hefei 230027, China;

Abstract: Accurate modeling of thermal characteristics is critical to the safe use and reliable management of lithium-ion batteries. However, limitations in sensors and testing methods make online real-time acquisition of internal temperatures extremely difficult. This paper uses the similarity of dynamic system modeling to construct a lumped thermal characteristic model of the battery. By analyzing the heat conduction mechanism inside the battery, the optimized heat path model is combined with the classical Bernardi equation to realize the state description of the battery thermal characteristic system. In addition, the forgetting factor recursive least squares algorithm is used to realize the online identification of the parameters of the lumped thermal characteristics model. Meanwhile, the identification of the external thermal resistance is coupled with the estimation of the internal temperature, and a novel online adaptive co-estimation strategy based on the forgetting factor recursive least squares - joint Kalman filter is proposed, which solves the problem that the external thermal resistance cannot be accurately identified adaptively in a complex environment. The experimental results show that the maximum root-mean-square error of the model under different experiments is 0.53°C, which verifies the high-accuracy of the lumped thermal characteristics modeling strategy.

*Corresponding author: *Shunli Wang. Tel/fax: +86-15884655563. E-mail address: wangshunli@swust.edu.cn.*

1. Introduction

In recent years, benefiting from the explosive development of the global new energy vehicle industry, lithium-ion batteries have rapidly become the mainstream power source by virtue of their high energy density and long cycle life [1, 2]. Compared with aging, self-discharge and capacity decline and other defects of their own, the safety problems caused by the difficulty of real-time prediction of battery temperature status have seriously restricted the scale development of new energy vehicles [3]. Therefore, the thermal characteristics modeling of the power battery and the high-precision prediction of the internal temperature are essential to prevent battery thermal runaway and ensure safe and long-life operation. In addition, for battery thermal management systems, different thermal management systems may have different temperature control methods, which in turn causes different battery thermal management systems to have different external heat transfer coefficients [4]. Using the same external heat transfer coefficient under different working conditions will increase the error of the internal temperature estimation of the battery [5]. Therefore, the adaptive working condition prediction method of the external heat transfer coefficient of the battery is extremely important for the high-accuracy thermal characteristic modeling and the construction of an efficient thermal management system.

The complex internal structure and changeable application environment of lithium-ion batteries make it easy to produce uneven internal temperature distribution and higher internal temperature during use, which increases the difficulty of estimating the internal temperature of the battery [6, 7]. For the thermal characteristics modeling of power lithium-ion batteries, different modeling methods often have

differences in reliability and accuracy [8-10]. At present, the commonly used internal temperature measurement of batteries includes experimental internal temperature measurement methods, offline internal temperature prediction methods, and battery internal temperature estimation methods based on online estimation. The internal temperature measurement method based on experiments is usually to embed a thermocouple inside the battery [11-15]. This method is only suitable for testing the relevant thermal characteristics of the battery under experimental environmental conditions. In the actual application of the battery, the feasibility of this method is low and there are huge hidden dangers in the long-term use of the battery, and the safety problem of the battery in use cannot be guaranteed. The offline-based internal temperature prediction usually uses finite element numerical calculation methods. By establishing a battery cell thermal model and performing offline simulation, the internal temperature of the battery is estimated [16-20]. This method is mainly used for battery cell packaging design and module design, and the finite element numerical calculation method has extremely high computational complexity, and is not suitable for the practical application and thermal management of batteries.

The above related battery internal temperature research is based on the laboratory or offline, and the development of an application-level vehicle battery thermal management system needs to meet the online estimation of the battery internal temperature. The method of predicting the internal temperature of the battery based on online estimation often takes practical application as the starting point to realize the thermal management of the battery [21-23]. Based on online estimation of battery internal temperature prediction methods can be roughly divided into DC internal resistance method, electrochemical impedance spectroscopy (EIS) measurement analysis method and temperature difference transfer function method. Li et al [24] and Howey et al [25] conducted related studies on the DC internal resistance method, which uses the DC internal resistance as a function of the internal and external temperature of the battery to estimate the internal temperature of the battery by looking up tables

or functional calculations. However, because different types of batteries, or different batteries of the same type, have different functional relationships between the DC internal resistance and the internal and external temperature of the battery, the DC internal resistance method does not have universal application. In addition, scholars in the field have also studied the EIS measurement and analysis method [26-28]. The principle of this method is similar to the DC internal resistance method. Using the corresponding function relationship between the general amplitude and phase angle of the battery's AC impedance and the internal temperature of the battery, the internal temperature of the battery can be estimated by looking up a table or function calculation [29, 30]. However, due to the harsh requirements of the working environment and the high price of the EIS measuring instrument, it is not suitable for practical applications in automobiles. In view of the obvious drawbacks of the above-mentioned internal temperature estimation methods, in order to improve the reliability of battery thermal modeling, related researchers applied the temperature difference transfer function method based on thermal circuit network modeling [31, 32]. This method uses the transfer function between the internal temperature of the battery and the heating power of the system, and calculates the internal temperature of the battery through the input current of the system [33-35]. The temperature difference transfer function method is more commonly used in current battery internal temperature estimation, but this method is an open-loop estimation, and cannot adaptively update the parameters of the transfer function according to changes in the external environment, and the accuracy is low.

In addition to the above-mentioned battery thermal characteristics modeling methods, related scholars in the field have done related work on battery thermal management and internal temperature estimation research, and have achieved good results to a certain extent. Saw et al. [36] proposed a new thermal management system using mist cooling to keep the surface temperature of the battery module below 40°C, and verified through experiments and data that the mist cooling method is an effective

thermal management for lithium-ion battery packs. plan. Liu et al. [37] used dual-particle filtering to complete the temperature compensation modeling of the power lithium-ion battery, and solved the disturbance effect of the drift current on the model parameters. Xu et al. [38] constructed a new type of computational fluid dynamics model of the cooling system to keep the maximum temperature inside the battery below 32.5°C and improve the uniformity of temperature distribution between battery cells. On the basis of clarifying the internal heat transfer and heat generation mechanism of the battery, Jiang et al. [39] proposed a battery charge-discharge cycle thermal management model based on heat pipes and phase change materials to ensure that the battery has a lower temperature environment during long-term cycles. Liang [40] and others established a two-dimensional heat circuit network model, and based on this model, solved the heat generation and heat transfer mechanism of the battery. Chen [41] et al. established a new battery thermoelectric coupling model by considering the internal gelatinous structure of the battery and the high current and situation caused by external short circuit, and controlled the internal temperature and surface temperature error during short circuit within 1.771% and 3.915%, respectively. Despite the increasing research work on thermal management systems in academia, its main work focuses on the thermal cooling system and internal temperature estimation of the battery. The thermal management approach based on the battery cooling system can only control the battery within a certain temperature range to a certain extent, and the construction of the cooling system will increase the degree of coupling between the battery management system, which is extremely costly in the long-term use of the battery.

Based on the above discussion, the high computational complexity or harsh environmental conditions of use have kept most of the research in the laboratory stage and prevented the implementation of the system for practical on-board applications. In addition, the problem of uncertainty of external thermal resistance in modeling the battery thermal circuit system and the inability of adaptive accurate

estimation of internal temperature under variable environments have not received sufficient attention. In this paper, aiming at the problem that the internal temperature of the battery is difficult to self-adaptively and accurately estimate online, a lumped thermal characteristic model (LECM) based on circuit theory is established. Meanwhile, by analyzing the internal heat generation and heat dissipation mechanism of the battery, the discrete state-space equation expression of the thermal characteristic model is realized. Finally, considering the uncertainty of external thermal resistance, an idea of estimation strategy based on the adaptive forgetting factor least squares - joint Kalman filter (AFFRLS-JKF) is proposed to achieve the adaptive cooperative estimation of the full-parameter of LTCM and the internal temperature of the battery. The experiment verifies the high-accuracy of the LECM and the high-precision of the AFFRLS-JKF estimation strategy.

2. Mathematical analysis

2.1. Lumped thermal characteristic modeling

From the perspective of modeling the system, physical systems of the same order have similar dynamic characteristic equations. Therefore, based on the similarity between the total electric property modeling and the thermal property modeling of the battery, the thermal property network of the single battery cell is described by an equivalent electric property network to realize the total parameter thermal property modeling of the lithium-ion battery. The current source, capacitance and resistance of the electrical characteristic network are equivalent to the thermal power, heat capacity and thermal resistance of the thermal characteristic network, respectively. It is worth noting that thermal property modeling is always coupled with the electrical property parameter identification and internal state estimation algorithm of the battery throughout the online long-term application of the BMS. For this reason, while ensuring the accuracy of the battery temperature state estimation, its internal temperature estimation

should keep the computational complexity of the battery management system (BMS) low. In view of the fact that the information provided by the external characteristics of the battery is necessary for the subsequent internal temperature estimation online embedded application research, this paper assumes that the battery cell is a uniform heat generating body with the highest temperature at the center of the battery. Based on the above assumptions and online application requirements, with the goal of modeling and solving the thermal characteristics of power batteries, the lumped thermal characteristics model (LTCM) of the battery is constructed in a targeted manner. The simplified battery lumped thermal characteristic model is shown in Fig. 1.
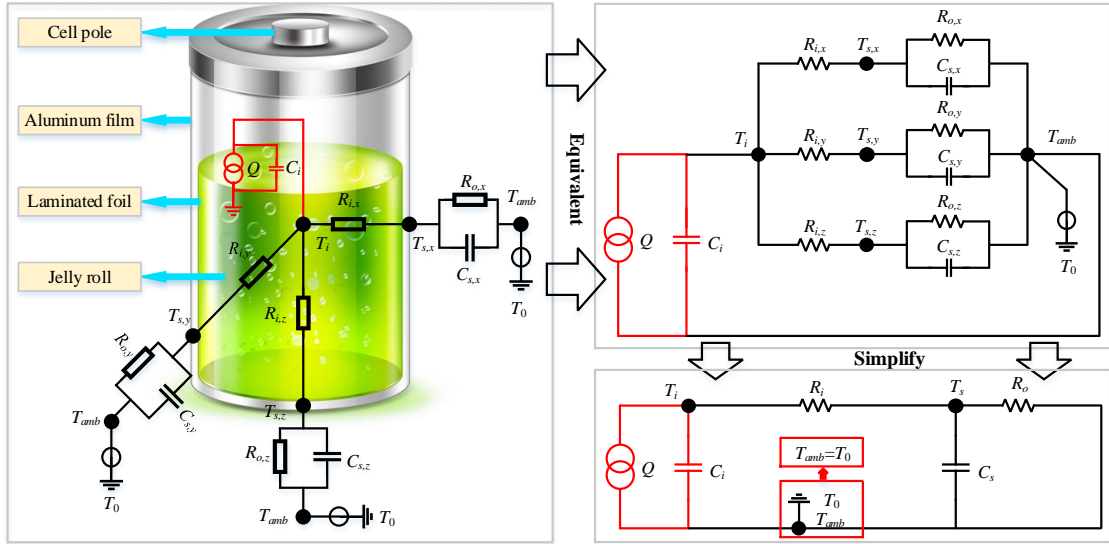

Fig. 1. LTCM structure and simplified mechanism

The Fig.1 (a) shows the physical modeling framework of a cylindrical lithium-ion battery. The Fig. 1(b) shows the equivalent structure of the cylindrical lithium-ion battery's thermal characteristics modeling. The Fig. 1(c) is a simplified structure for modeling the thermal characteristics of a cylindrical lithium-ion battery. In Fig.1(a), Q is the total heating power of the battery. There are two ways to conduct it: one part heats the battery, and the other part conducts to the outside via thermal resistance. T_i is the highest point in the center of the battery. T_s is the temperature of the battery surface area. T_{amb} is the ambient temperature where the battery is located. T_0 is the model reference temperature point. Generally,

T_{amb} is set as the external reference temperature point. $R_{i,x}$, $R_{i,y}$ and $R_{i,y}$ are the thermal resistances in various directions inside the battery, which are related to the thermal conductivity inside the battery. $R_{o,x}$, $R_{o,y}$, and $R_{o,z}$ are the thermal resistance in various directions outside the battery, and are related to the heat transfer coefficient outside the battery. C_i is the equivalent heat capacity inside the battery. C_s is the equivalent heat capacity of the battery casing. It is worth noting that the cylindrical battery sample used in this test is an aluminum case with excellent thermal conductivity, and the heat capacity of the case is extremely small. Therefore, while ensuring the accuracy of the model as much as possible, the entire lumped parameter thermal characteristic model can be simplified. The simplified LTCM model structure is shown in Fig.1(C). Based on this, this research will realize the modeling and solving of the thermal characteristics of the battery.

2.2. Model-based time domain analysis

The calculation of battery heat generation is the basis of the entire lumped thermal characteristics modeling. Understanding the battery heat generation mechanism is crucial to the accurate solution of LTCM. Different charging and discharging current rates of the battery will cause the battery to produce a time-varying heat production rate, which in turn causes the temperature difference between the battery core and the casing. In addition, the inherent internal resistance of the battery is also one of the essential reasons for the heat generation of the battery. Therefore, when modeling the heating power of the battery, the influence of current and internal resistance on the heating power should be considered. To accurately calculate the heat generation power of the cell requires consideration of the reaction heat, polarization heat and Joule heat of the cell. The calculation formula is shown in Equation (1).

$$Q = Q_p + Q_j + Q_r + Q_s \tag{1}$$

In Equation (1), Q_p is the heat of polarization, Q_j is the Joule heat, Q_r is the heat of reaction, and Q_s

is the heat of side reaction. Through the analysis of the heat source mechanism, it can be known that both Q_p and Q_j are positive when the battery is charged and discharged. Q_r is negative when the battery is charging, and positive when the battery is discharging. In addition, Q_s is related to the electrode decomposition that occurs during self-discharge of the battery, and the heat is very small during charging and discharging, so it can be ignored. With the goal of reducing the computational complexity of the model, the heat generation and heat dissipation mechanism of the battery is studied through the method of lumped parameter modeling. The Bernardi equation is used to calculate the equivalent heating power of the battery, as shown in Equation (2).

$$Q \approx \underbrace{I\left(E - U_L\right)}_{Q_p + Q_j} + \underbrace{IT\left(dE\right)/dT}_{Q_r} \qquad (2)$$

In Equation (2), I is the charge and discharge current of the battery. T is the battery temperature. E is the internal balance electromotive force of the battery. U_L is the terminal voltage of the battery. dE/dT represents the entropy thermal coefficient of the battery, that is, the coefficient of the reversible reaction of the battery. The classic Bernardi equation contains more inputs, which is not conducive to the application of embedded systems. In order to reduce the calculation complexity of the battery heat source, the Bernardi heating power equation is further simplified according to Kirchhoff's law, and the simplified heating power calculation expression of the lumped parameter thermal model of the battery is obtained, as shown in Equation (3).

$$Q \approx I^2 R_s + IT\left(dE\right)/dT \Leftarrow E - U_L = IR_s \qquad (3)$$

In Equation (3), R_s represents the internal DC resistance of the battery. By clarifying the shunt mode of heating power in LTCM, the similarity of system modeling is used to express the time-domain state-space equation of the thermal characteristic model. First, based on Bernardi's simplified equation, combined with Kirchhoff's circuit law in circuit science, the differential equations of T_i node and T_s node

are derived, as shown in Equation (4).

$$\begin{cases} \dfrac{dT_{is}}{dt} = -\dfrac{1}{R_i C_i} T_{is} + \dfrac{1}{R_i C_i} T_{ss} + \dfrac{Q}{C_i} \\ \dfrac{dT_{ss}}{dt} = \dfrac{1}{R_i C_s} T_{is} + \left(\dfrac{1}{R_i C_s} + \dfrac{1}{R_o C_s} \right) T_{ss} \end{cases} \Leftarrow \begin{cases} T_{is} = T_i - T_{amb} \\ T_{ss} = T_s - T_{amb} \end{cases} \tag{4}$$

In Equation (4), T_{is} is the difference between the internal temperature of the battery and the

reference temperature point, and T_{ss} is the difference between the surface temperature of the battery and

the reference temperature point. In theory, state variables are not required to be physically measurable.

In this paper, T_{is} and T_{ss} are selected as the state variables of the system, and the heating power Q is the

input vector of the system. Based on the heat prevalence law of the lumped parameter thermal model,

the state equation of the battery thermal circuit system is established to describe the dynamic

characteristics of the thermal circuit of the model. The expression form of the state equation in the time

domain state is shown in Equation (5).

$$\underbrace{\begin{bmatrix} \dot{T}_{is} \\ \dot{T}_{ss} \end{bmatrix}}_{\dot{x}_t} = \underbrace{\begin{bmatrix} -\dfrac{1}{R_i C_i} & \dfrac{1}{R_i C_i} \\ \dfrac{1}{R_i C_s} & -\left(\dfrac{1}{R_i C_s} + \dfrac{1}{R_o C_s} \right) \end{bmatrix}}_{A_t} \underbrace{\begin{bmatrix} T_{is} \\ T_{ss} \end{bmatrix}}_{x_t} + \underbrace{\begin{bmatrix} \dfrac{1}{C_i} \\ 0 \end{bmatrix}}_{B_t} \underbrace{[Q]}_{u_t} \tag{5}$$

In equation (5), x_t is the system state variable in continuous state, which is composed of the highest

internal temperature T_{in} and the battery surface area temperature T_{ss}. u_t is the input vector of the system

in continuous state. $\dot{x}_t$ is the differential form of the system state variable. A_t is the system matrix in

the time domain state, and B_t is the control matrix in the continuous state. In the optimal control of

engineering practice, state variables are often required as feedback variables, and choosing easy-to-

measure physical variables as state variables is beneficial to the iterative identification of the system. In

the embedded system application of lithium-ion battery, the value of T_{ss} is easier to measure safely than

T_{in}. Therefore, this paper selects T_{ss} as the output vector of the battery thermal circuit system to obtain

the observation equation under the continuous time state, as shown in Equation (6).

$$T_{ss} = \underbrace{\begin{bmatrix} 0 & 1 \end{bmatrix}}_{C_t} \underbrace{\begin{bmatrix} T_{is} \\ T_{ss} \end{bmatrix}}_{x_t} + \underbrace{\begin{bmatrix} 0 \end{bmatrix}}_{D_t} \underbrace{\begin{bmatrix} Q \end{bmatrix}}_{u_t} \tag{6}$$

In Equation (6), y_t is the output vector of the system in the time domain state. $\mathbf{C}_t$ is the output matrix in the time domain state. $\mathbf{D}_t$ is the direct transfer moment matrix in the time domain state. In particular, in the state-space equation of the heat circuit system, the output vector is directly reflected by the output matrix, and the direct transmission of the input vector is not considered, that is, $\mathbf{D}_t=0$.

2.3. Online identification of thermal circuit model parameters

The identification of thermal characteristic parameter values is the basis for high-precision estimation of the internal temperature of lithium-ion batteries. Aiming at the embedded system application of thermal characteristics modeling, this paper uses transfer function instead of differential equation to describe the thermal characteristics of LTCM. First, with the goal of deriving the exogenous autoregressive model of the system, the complex frequency domain equation of the lumped parameter thermal model is obtained by using the Laplace transform rule. As shown in Equation (7).

$$\begin{cases} sT_{is}(s) = -\dfrac{1}{R_i C_i} T_{is}(s) + \dfrac{1}{R_i C_i} T_{ss}(s) + \dfrac{Q(s)}{C_i} \\ sT_{ss}(s) = \dfrac{1}{R_i C_s} T_{is}(s) + \left(\dfrac{1}{R_i C_s} + \dfrac{1}{R_o C_s} \right) T_{ss}(s) \end{cases} \tag{7}$$

In Equation (7), s is the Laplace operator. By further transforming the complex frequency domain equation of the T_i node in Equation (7), the coupling relationship between the surface temperature T_{ss} in the frequency domain, the maximum internal temperature T_{is} and the heating power Q of the system is obtained. As shown in Equation (8).

$$T_{ss}(s) = T_{is}(s) - R_i \left[Q(s) - C_i s T_{is}(s) \right] \tag{8}$$

The relationship equations between T_{ss}, T_{is} and Q are brought into the complex frequency domain

equation of the T_s node, and then the functional equation containing only the maximum internal temperature T_{is} and the heating power Q of the system is obtained. Then, the functional equation containing only T_{is} and Q is further transformed, and the heating power Q is used as the system input, and the internal maximum temperature T_{is} is used as the system output to obtain the system transfer function based on LTCM. As shown in Equation (9).

$$G(s) = \frac{1 + R_i/R_o + C_s R_i s}{C_s C_i s^2 + (C_s + C_i + R_i C_i/R_o)s + 1/R_o} \Leftarrow G(s) = \frac{T_{is}(s)}{Q(s)} \tag{9}$$

The Equation (9) derives the functional relationship between the heating power Q and the maximum internal temperature T_{is}, and the heating power Q can be approximated by Equation (3). Therefore, combining these two equations can complete the approximate estimation of the internal temperature, but it cannot realize the adaptive adjustment of the parameters and the temperature state. In addition, the model equations in the complex frequency domain are only suitable for laboratory research and cannot realize online applications of embedded systems. In view of the above-mentioned problems, the Equation (9) is further discretized using Z-transform and Z-inverse transformation theory, and the difference equation form of the thermal circuit system in the time domain is obtained. As shown in Equation (10).

$$T_{is,k+2} = \alpha_1 T_{is,k+1} + \alpha_2 T_{is,k} + \beta_1 Q_{k+1} + \beta_2 Q_k \tag{10}$$

In Equation (10)，α_1, α_2, β_1, and β_2 are parameters to be identified. The derivation of α_1, α_2, β_1, and β_2 calculation is shown in Equation (11).

$$\begin{cases} \alpha_1 = -\Delta t/R_i C_i - \Delta t/R_o C_s - \Delta t/R_i C_s + 2 \\ \alpha_2 = (1 - \Delta t/R_i C_i)(\Delta t/R_o C_s + \Delta t/R_i C_s - 1) \\ \beta_1 = \Delta t/C_i , \beta_2 = (\Delta t/C_i)(\Delta t/R_o C_s + \Delta t/R_i C_s - 1) \end{cases} \tag{11}$$

It should be noted that there are three linearly independent equations in Equation (11), and there are four thermal characteristic parameters that need to be identified in LTCM, namely C_i, R_i, C_s and R_o.

This means that Equation (11) is an underdetermined equation, but only a well-determined equation or an overdetermined equation can solve the unique parameter value. Taking into account the uncertain characteristics of the R_o value of the battery's external equivalent thermal resistance, when identifying the parameters in the LTCM, this paper couples R_o with the state variables of the thermal circuit system to achieve an adaptive collaborative estimation of the internal temperature and R_o.

$$\begin{cases} C_i = \Delta t/\beta_1, R_i = (\beta_1\beta_2)/(\beta_2 - \alpha_2\beta_1) \\ C_s = (\Delta t\beta_1)/R_o + \Delta t(\alpha_1 - 2) - \Delta t/\beta_1 \end{cases} \tag{12}$$

What needs to be explained is that whether it is a battery cell or a battery pack, the value of the corresponding internal maximum temperature point T_{is} under different current conditions is not easy to obtain. The reason why this paper uses the difference equation of heating power Q and internal maximum temperature T_{is} to identify the parameters of the thermal circuit model is as follows.

i   The values of the thermal characteristic parameters C_i, R_i and C_s of the battery LTCM are related to the material of the battery and will not change with the change of the input current of the system.

ii   The internal temperature estimation value of the battery needs to be analyzed for error with the internal temperature measurement value, and this research has obtained the internal temperature value of the battery in advance during the experiment.

2.4. Discretization analysis of state-space equations

The discretized expression of the state estimation equation is the basis for the simulation verification of the battery thermal characteristic modeling and the later embedded online application. Using the similarity of physical systems, combined with Bernardi simplified equations, the state-space equation of the model in the time domain state is obtained. However, from the perspective of engineering practice, the state equation description of the heat circuit model in the time domain state is not suitable for online temperature estimation applications. Therefore, it is necessary to discretize the state-space

equation in the above-mentioned time-domain state. First, the matrix differential equations are used to replace the matrix differential equations of the T_i node and the T_s node, as shown in Equation (13).

$$\begin{cases} \dot{T}_{is} = \left(T_{is,k+1} - T_{is,k}\right)/\Delta t \\ \dot{T}_{ss} = \left(T_{ss,k+1} - T_{ss,k}\right)/\Delta t \end{cases} \tag{13}$$

In Equation (13), k represents a discrete time variable. t represents a continuous time variable. $T_{is,k}$ and $T_{is,k+1}$ respectively represent the temperature value of the highest temperature point inside the battery at time k and $k+1$. $T_{ss,k}$ and $T_{ss,k+1}$ respectively represent the temperature value of the highest temperature point on the battery surface at time k and $k+1$. Δt represents the sampling time of the system. Aiming at the online estimation target of the internal temperature state of the power battery, combined with the first-order forward difference equation, the discretization of the time-domain state-space equation is completed. The overall discretization process is shown in the following Equation (14).

$$\begin{cases} \dot{x}_t = \boldsymbol{A}_t x_t + \boldsymbol{B}_t u_t \\ y_t = \boldsymbol{C}_t x_t + \boldsymbol{D}_t u_t \end{cases} \overset{\Delta}{\Longrightarrow} \begin{cases} x_{d,k+1} = f(x_{d,k}, u_k) + w_k \approx \boldsymbol{A}_d x_{d,k} + \boldsymbol{B}_d u_k + w_k \\ y_k = h(x_{d,k}, u_k) + v_k \approx \boldsymbol{C}_d x_{d,k} + \boldsymbol{D}_d u_k + v_k \end{cases} \tag{14}$$

In Equation (14), $x_{d,k}$ and $x_{d,k+1}$ are the state variables of the system at time k and $k+1$ in the discrete state, respectively. y_d is the output vector of the system in the discrete state. u_k is the input of the system at the current moment. $\boldsymbol{A}_d$ is the system matrix in the discrete state. $\boldsymbol{B}_d$ is the control matrix in the discrete state. $\boldsymbol{C}_d$ is the observation matrix in the discrete state. $\boldsymbol{D}_d$ is the direct transfer moment matrix in the discrete state. Since the discrete state-space equation of the thermal circuit system does not consider the direct transmission of the input vector, that is, $\boldsymbol{D}_d=0$. w_k and v_k are system noise and observation noise respectively. Expand the discrete state-space equations to get the system discrete state equations based on LTCM as Equation (15).

$$\underbrace{\begin{bmatrix} T_{is,k+1} \\ T_{ss,k+1} \end{bmatrix}}_{x_{d,k+1}} = \underbrace{\begin{bmatrix} 1 - \dfrac{\Delta t}{R_i C_i} & \dfrac{\Delta t}{R_i C_i} \\ \dfrac{\Delta t}{R_i C_s} & 1 - \left(\dfrac{\Delta t}{R_i C_s} + \dfrac{\Delta t}{R_o C_s} \right) \end{bmatrix}}_{A_d} \underbrace{\begin{bmatrix} T_{is,k} \\ T_{ss,k} \end{bmatrix}}_{x_{d,k}} + \underbrace{\begin{bmatrix} \dfrac{\Delta t}{C_i} \\ 0 \end{bmatrix}}_{B_d} \underbrace{[Q_k]}_{u_k} + \underbrace{\begin{bmatrix} w_k^1 \\ w_k^2 \end{bmatrix}}_{w_k} \tag{15}$$

In Equation (15), the heating power Q_k is the input value of the system at time k. Taking the surface temperature T_{ss} of the lithium-ion battery as the observation variable, based on the lumped thermal characteristic modeling theory, the observation equation under the discrete state based on LTCM is obtained, as shown in Equation (16).

$$\underbrace{T_{ss,k+1}}_{y_k} = \underbrace{\begin{bmatrix} 0 & 1 \end{bmatrix}}_{C_d} \underbrace{\begin{bmatrix} T_{is,k} \\ T_{ss,k} \end{bmatrix}}_{x_{d,k}} + \underbrace{[0]}_{D_d} \underbrace{[Q_k]}_{u_k} \tag{16}$$

2.5. Adaptive temperature and parameter co-estimation strategy

The parameter identification of LTCM is the basis for realizing the internal temperature estimation of the battery. Regarding the thermal management of the battery, because different thermal management systems may have different temperature control methods, different battery thermal management systems have different external heat transfer coefficients. This leads to the uncertainty of the R_o value of the external equivalent thermal resistance of the battery in different use environments. When the use environment of the battery changes, if the originally identified parameter values of the thermal circuit model are still used, the estimation error of the internal temperature of the battery will inevitably increase. In order to solve the above uncertainty problem of R_o, this paper uses FFRLS algorithm to identify the thermal parameters of LTCM online. At the same time, the identification of the external equivalent thermal resistance R_o is coupled with the estimation of the internal temperature of the battery, and an adaptive co-estimation strategy of the external equivalent thermal resistance R_o and the internal temperature state T_{is} based on AFFRLS-JKF is proposed. The AFFRLS-JKF adaptive collaborative

estimation strategy makes up for the disadvantage that the FFRLS algorithm cannot adaptively modify

the R_o value of the external equivalent thermal resistance. The iterative framework of using AFFRLS-

JKF estimation strategy to realize the parameter identification of LTCM and the joint estimation of
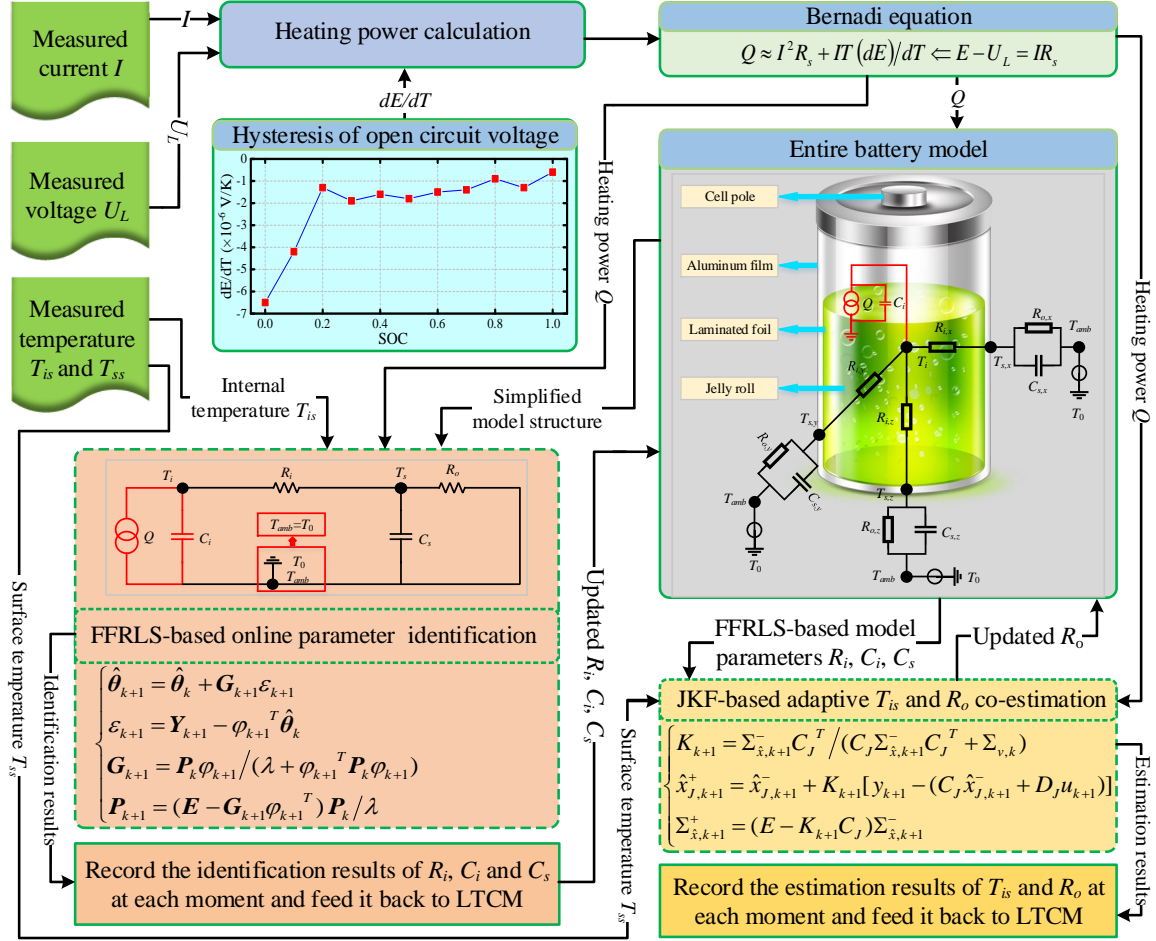
internal temperature is shown in Fig. 2.

Fig. 2 Online temperature and parameter co-estimation framework based on AFFRLS-JKF strategy

It can be seen from Fig. 2 that based on the exogenous autoregressive model [42], the FFRLS

algorithm is used to identify the values of C_i, R_i, and C_s in the LTCM, and the JKF algorithm is used to

realize the adaptive collaborative prediction of the internal temperature state T_{is} and the external thermal

resistance R_o. First, the difference equation form of the single-input single-output system shown in

Equation (10) is further modified to obtain an exogenous autoregressive model form suitable for the

online iterative form, as shown in Equation (17).

$$Y = \varphi^T \theta \Leftarrow \begin{cases} \theta = [\alpha_1, \alpha_2, \beta_1, \beta_2]^T \\ \varphi = \{\varphi_0, \varphi_1, \varphi_2, \cdots, \varphi_k, \cdots, \varphi_{n-2}\} \\ Y = [T_{is,2}, T_{is,3}, T_{is,4}, \cdots, T_{is,k+2}, \cdots, T_{is,n}]^T \\ \varphi_k = [T_{is,k+1}, T_{is,k}, Q_{k+1}, Q_k]^T \end{cases} \tag{17}$$

In Equation (17), Y represents the output matrix of the exogenous autoregressive model. φ is the data matrix, and θ is the coefficient matrix. Based on the exogenous autoregressive model, the parameter solution of LTCM is realized. The main steps of the LTCM parameters identified by the FFRLS algorithm are as follows.

Step 1: Assign an initial value to k, and initialize the coefficient matrix $\hat{\theta}_0$ and error covariance matrix P_0.

$$\begin{cases} k = 0, \hat{\theta}_0 = E[\theta_0] \\ P_0 = E[(\theta_0 - \hat{\theta}_0)(\theta_0 - \hat{\theta}_0)^T] \end{cases} \tag{18}$$

Step 2: Read the data matrix φ_{k+1} at time $k+1$, and calculate the gain matrix G_{k+1}.

$$G_{k+1} = P_k \varphi_{k+1} / (\lambda + \varphi_{k+1}^T P_k \varphi_{k+1}) \tag{19}$$

Step 3: Update the error covariance matrix P_{k+1} at time $k+1$.

$$P_{k+1} = (E - G_{k+1}\varphi_{k+1}^T) P_k / \lambda \tag{20}$$

Step 4: Calculate the coefficient matrix $\hat{\theta}_{k+1}$ at time $k+1$.

$$\begin{cases} \hat{\theta}_{k+1} = \hat{\theta}_k + G_{k+1}\varepsilon_{k+1} \\ \varepsilon_{k+1} = Y_{k+1} - \varphi_{k+1}^T \hat{\theta}_k \end{cases} \tag{21}$$

Step 5: Use Equation (12) to calculate the parameters of LTCM.

Step 6: *Step* 2 to *step* 5 loop iterative calculations until the end of the full time series.

In Equations (10) to (21), P_{k+1} is the error covariance matrix of the coefficient matrix at $k+1$. G_{k+1} is the gain matrix of the FFRLS algorithm at $k+1$. ε_{k+1} is the innovation value at $k+1$, which represents the error value between the measured value and the estimated value of the highest internal temperature of the battery. λ is the forgetting factor of the algorithm, and the value of the forgetting factor in this

work is $\lambda=0.97$. Through Equation (3) we can get the value of the heating power Q of the battery LTCM. Similarly, using the data matrix $\boldsymbol{\varphi}_k = [T_{is,k+1}, T_{is,k}, Q_{k+1}, Q_k]^T$ input by the system, the value of the coefficient matrix is obtained under the iterative calculation of FFRLS. The parameter values of LTCM are further obtained by Equation (12).

The FFRLS algorithm gives the identification results of C_i, R_i and C_s in LTCM, but it cannot adaptively identify the value of the external thermal resistance R_o in LTCM. Therefore, considering the uncertainty of the value of the external equivalent thermal resistance R_o, this paper is based on the JKF algorithm to realize the adaptive joint estimation of the external equivalent thermal resistance R_o and the internal temperature state T_{is}. The JKF algorithm uses R_o as one of the position state variables of the system, and realizes the adaptive identification of R_o through an online state estimation algorithm. Considering that the external equivalent thermal resistance R_o will be affected by the system's uncertain disturbance noise during identification, the system state-space equation of the external equivalent thermal resistance R_o is given, as shown in Equation (22).

$$R_{o,k+1} = R_{o,k} + r_k \tag{22}$$

The Equation (22) describes the dynamic change process of the external equivalent thermal resistance R_o. Among them, r_k represents the disturbance noise of the system. Combining the system state equation describing the external equivalent thermal resistance with the system state-space equation describing the temperature state, a JKF algorithm suitable for adaptive collaborative estimation of the battery external equivalent thermal resistance and internal temperature is constructed, as shown in Equation (23).

$$\begin{cases} x_{J,k+1} = f(x_{J,k}, u_k) + w_k \approx \boldsymbol{A}_J x_{J,k} + \boldsymbol{B}_J u_k + w_k \\ y_k = h(x_{J,k}, u_k) + v_k \approx \boldsymbol{C}_J x_{J,k} + \boldsymbol{D}_J u_k + v_k \end{cases} \tag{23}$$

In Equation (23), $x_{J,k}$ is a three-dimensional system matrix, and the matrix is denoted as

$x_J = \begin{bmatrix} T_{is} & T_{ss} & R_o \end{bmatrix}^T$. u_k is the input vector of the system, and the matrix is expressed as $u_k = Q_k$. y_k is the output vector of the system, and the matrix is expressed as $y_k = T_{ss,k}$. A_J is the system matrix, B_J is the control matrix, C_J is the output matrix, and D_J is the direct connection matrix. The matrix representation of A_J, B_J, C_J and D_J is shown in Equation (24).

$$\begin{cases} A_J = \begin{bmatrix} A_d & 0 \\ 0 & 1 \end{bmatrix} & B_J = [\Delta t / C_i \quad 0 \quad 0]^T \\ C_J = [0 \quad 1 \quad C_3] & D_J = [0] \end{cases} \tag{24}$$

In Equation (24), C_3 is used to describe the relationship between the surface area temperature T_{ss} and the external thermal resistance R_o, and its value is obtained by obtaining the partial derivative of the observation equation. The calculation equation of C_3 is shown in Equation (25).

$$C_3 = \frac{\partial h(x_{J,k}, u_k)}{\partial R_o} = \frac{\partial h(x_{J,k}, u_k)}{\partial x_{J,k}} \cdot \frac{dx_{J,k}}{\partial R_o} = \frac{dT_{ss,k}}{dR_o} = \frac{\Delta t}{R_o^2 C_s} \tag{25}$$

The above Equations (23) to (25) derive the state-space equations for the adaptive co-estimation of the external equivalent thermal resistance and the internal temperature state. On this basis, the loop iteration body of the JKF algorithm suitable for online embedded applications is obtained. The main steps are as follows.

Step 1: Assign an initial value to k, and initialize the coefficient matrix and error covariance matrix.

$$\begin{cases} k = 0, \hat{x}_0^+ = E[x_0] \\ \Sigma_{\hat{x},0}^+ = E[(x_0 - \hat{x}_0^+)(x_0 - \hat{x}_0^+)^T] \end{cases} \tag{26}$$

Step 2: Time update of state variable estimates, as shown in Equation (37).

$$\hat{x}_{J,k+1}^- = A_J \hat{x}_{J,k}^- + B_J u_k \tag{27}$$

Step 3: Time update of error covariance matrix, as shown in Equation (31).

$$\Sigma_{\hat{x},k+1}^- = A_J \Sigma_{\hat{x},k}^+ A_J^T + \Sigma_{w,k} \tag{28}$$

Step 4: Calculate the Kalman gain matrix, as shown in Equation (32).

$$K_{k+1} = \Sigma_{\hat{x},k+1}^{-} C_J^{\,T} \Big/ (C_J \Sigma_{\hat{x},k+1}^{-} C_J^{\,T} + \Sigma_{v,k}) \tag{29}$$

Step 5: Measurement update of state variable estimates, as shown in Equation (33).

$$\hat{x}_{J,k+1}^{+} = \hat{x}_{J,k+1}^{-} + K_{k+1}[y_{k+1} - (C_J \hat{x}_{J,k+1}^{-} + D_J u_{k+1})] \tag{30}$$

Step 6: Measurement update of error covariance matrix, as shown in Equation (34).

$$\Sigma_{\hat{x},k+1}^{+} = (E - K_{k+1} C_J) \Sigma_{\hat{x},k+1}^{-} \tag{31}$$

Step 7: *Step* 2 to *step* 6 loop iterative calculations until the end of the full time series

In Equations (26) to (31), $\hat{x}_{J,k}^{-}$ is the prior state matrix at time k. $\hat{x}_{J,k}^{+}$ is posterior parameter estimate at time k, $\Sigma_{\hat{x},k}^{-}$ is the prior error covariance matrix of state variable at time k. $\Sigma_{\hat{x},k}^{+}$ is the posterior error covariance matrix of state variable at time k. K_k is the gain matrix at time k. $\Sigma_{w,k}$ and $\Sigma_{v,k}$ are the covariance of the system state error and the covariance of the observation error at time k, respectively. This paper uses the AFFRLS-JKF estimation strategy to realize the adaptive collaborative estimation of T_{is} and R_o. In addition, quantitative indicators are used to verify the accuracy of the lithium-ion battery LTCM and the precision of the AFFRLS-JKF estimation strategy. The application of related quantitative indicators is shown in Equation (32).

$$\text{RMSE} = \sqrt{\frac{1}{n}\sum_{i=1}^{n}(y_i - \hat{y}_i)^2}, \quad \text{MAPE} = \frac{1}{n}\sum_{i=1}^{n}\frac{|y_i - \hat{y}_i|}{y_i} \times 100\%, \quad \text{MAXE} = Max|y_i - \hat{y}_i| \tag{32}$$

In Equation (32), y_i and $\hat{y}_i$ represent the measured value and estimated value of the internal temperature, respectively. N is the total experiment time. The indicator RMSE stands for root-mean-square error, MAPE stands for mean-absolute-percentage error, and MAXE stands for maximum error.

3. Experimental analysis

3.1. Battery sample and experimental platform

To verify the accuracy of the LTCM and the accuracy of the AFFRLS-JKF algorithm under different working conditions, this research is based on the acquisition of internal temperature as the goal to conduct research and build a targeted experimental platform. The structure of the experimental platform is shown in Fig. 3. The experiment selects 18650 battery cells with $LiFePO_4$ as the battery sample. The detailed information of the battery sample is shown in Fig. 3(c). Before the experiment, the high-precision temperature sensor is connected to the electrode of the battery, and then the electrode of the battery is sealed with an adiabatic and insulating gel. Fix the connected battery with a special fixture to prevent the battery from moving during the experiment. In addition, the fixed battery samples are placed in a thermostat to ensure the stability of the ambient temperature and heat dissipation conditions. Finally, the battery sample is connected to a dedicated charging and discharging device, and the battery is subjected to charging and discharging experiments under different working conditions. Record and save the relevant experimental data on the host computer to complete the acquisition of data results under different experimental conditions. It should be pointed out that the proposed modeling strategy for the lumped thermal characteristics of batteries is general. However, due to the limitations of the existing laboratory conditions, this paper only selects 18650 battery cells with LiFePO4 as the battery sample for verification. The comparative verification study of batteries based on different chemical types will be further carried out in future work.
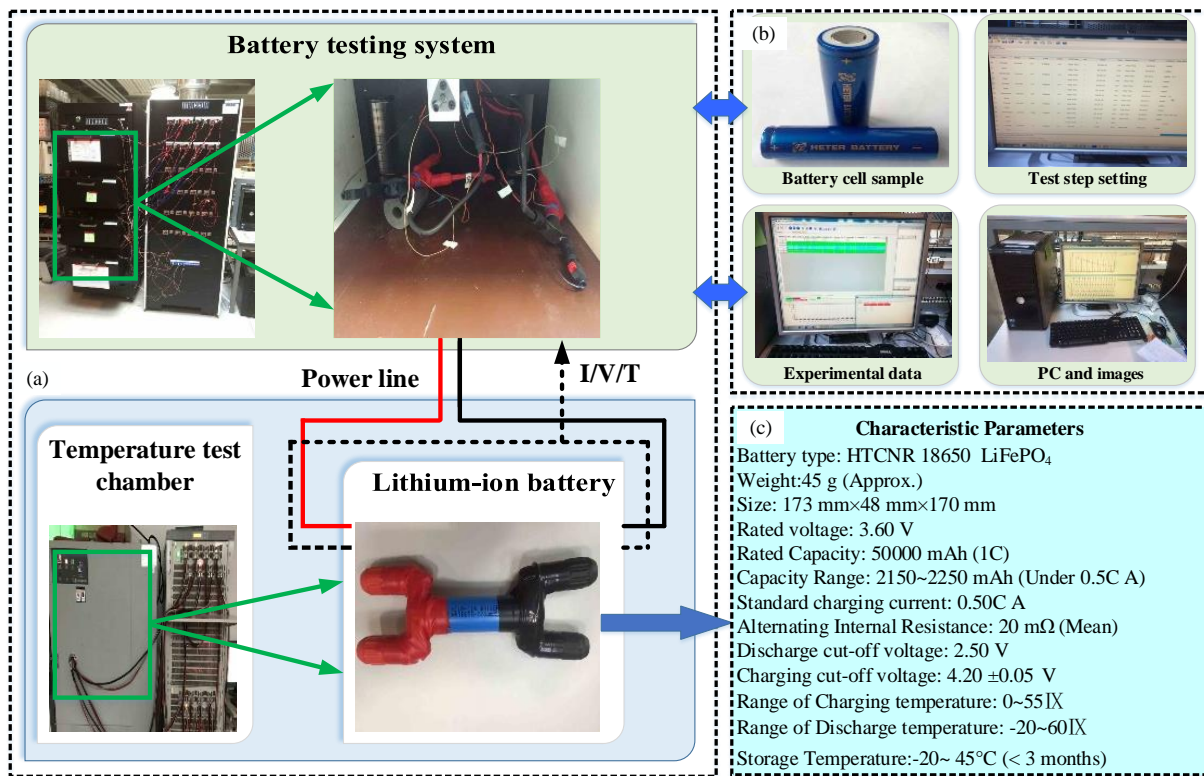
Fig. 3 Experimental platform and battery sample parameters

It should be noted that although the method of measuring the internal temperature of the battery with the built-in sensor has high measurement accuracy, the method with the built-in sensor will greatly increase the risk factor of the battery and is not suitable for the practical application of the battery. This paper regards the temperature of the sealed electrode as the internal temperature of the battery, ignoring the local heating caused by the connection of the battery poles, greatly improving the safety factor of the battery, and laying the foundation for the practical application of battery lumped thermal characteristics modeling.

3.2. Experimental results under different complex conditions

Based on the experimental platform built in the early stage, three different working conditions of hybrid pulse power characteristic cycle (HPPCC) experiment at constant 25℃, Beijing bus dynamic stress test cycle (BBDSTC) experiment at room temperature and full-charge and full-discharge test (FCFDT) experiment at constant 45℃ are designed and completed to measure the internal and external

temperature of the battery. Under the experimental data collected under the above working conditions, the accuracy of the LTCM model and the precision of the AFFRLS-JKF algorithm under different working conditions are verified.

3.2.1. CCDCT experiment at constant 25℃

In order to explore the adaptability of the model under constant temperature conditions and identify the definite parameters in LTCM, the HPPCC experiment at constant 25℃ is designed, and the thermal characteristic parameters of the battery under different discharge rates at 25℃ constant temperature are obtained. Before the experiment, put the battery in a thermostat with a temperature of 25°C and let it stand for 1 hour to make the battery's own temperature and the ambient temperature reach equilibrium. Then charge the battery with a constant current and voltage of 0.3 C to full charge, and then let it stand for 2 hours to balance the internal state of the battery. Next, load the battery with a 0.3 C pulse sequence to discharge the battery at a constant current. The duration of the constant current discharge pulse is 10 s and then stand for 40 s. Finally, use the same current pulse to charge the battery at a constant current for 10 s and then let it stand for 15 minutes. Use the same experimental procedure as above to perform hybrid-pulse-power-characteristic test on the battery with pulse sequences of 0.5 C, 1.0 C, 2.0 C and 2.0 C to achieve HPPC testing in a small cycle. Finally, discharge the battery with a current of 0.3 C for 10 minutes to ensure that the state of charge of the battery is reduced by 5%.

All the above-mentioned experimental steps constitute a large cycle. The HPPCC experiment designed in this paper has a large number of cycles M=20, and the entire experiment is carried out in a 25°C incubator. The CCDCT experimental process and experimental data are shown in Fig. 4. Among them, Fig.4(a) is the flow chart of the HPPCC experiment, and M in the figure represents the number of large cycles of the experiment. Fig. 4(b), Fig. 4(c) and Fig. 4(d) are the current curve, terminal voltage

curve and battery internal temperature curve of the HPPCC experiment, respectively.
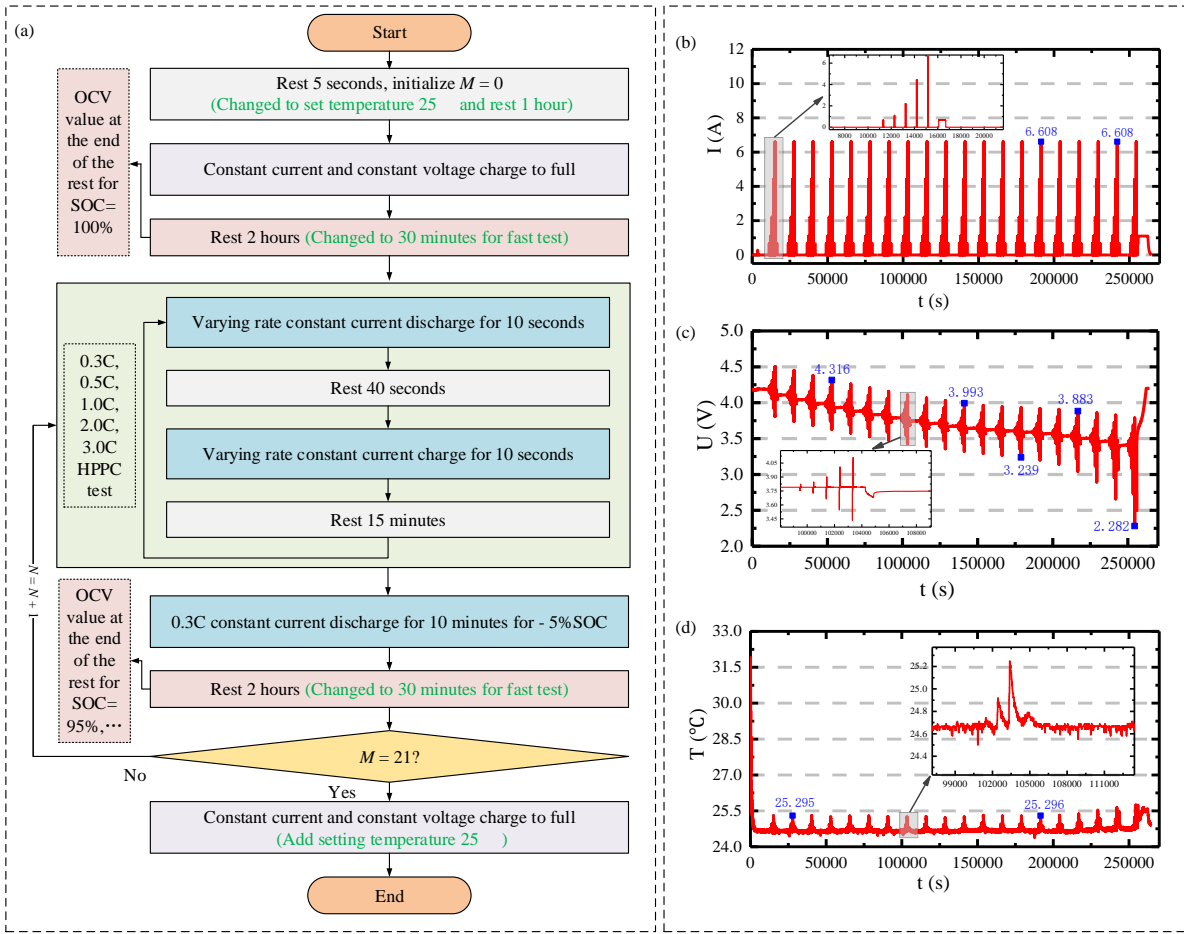

Fig. 4 CCDCT experimental process and experimental results

3.2.2. BBDSTC experiment at room temperature

The Beijing bus dynamic stress test (BBDST) experiment is an authoritative electric vehicle operating condition test experiment, which can be used to verify various performances of the BMS system. The average current used in the single-cycle BBDST experiment is 1 C, and the standard voltage of the battery sample is 3.6 V. According to the power calculation equation, the power value of battery power discharge can be calculated. The power time of a single BBDST experiment is about 300 s. In order to fully discharge the battery, a single experiment is carried out for 12 small cycles, and then the battery is charged at a constant current and voltage with a standard current of 0.5 C until the battery is fully charged. In order to fully simulate the complexity of the battery operating conditions, this paper

makes improvements on the basis of the BBDST experiment, taking 20 large cycles of the BBDST experiment as the battery temperature acquisition experiment, and the whole experiment is carried out in a constant temperature box. The BBDSTC experimental process and experimental results are shown in Fig. (5).

In Fig.5, N represents the number of small cycles in a single test. With a complete discharge in a single test as the goal, N=12 can be obtained by calculation. M represents the number of large cycles of the experiment, because the effective duration of a single data file stored in the experimental device is 3 days, and the test duration of a single BBDST is 3.5 hours, including pulse charge and discharge 1 hour and charge 2.5 hours. Therefore, after calculation, M=24×3/3.5≈20. Fig. 5(a) is the flow chart of the BBDSTC experiment. Fig. 5(b), Fig. 5(c) and Fig. 5(d) are the current curve, terminal voltage curve and battery internal temperature curve of the BBDSTC experiment, respectively. It should be noted that the entire experiment is carried out in an incubator that is not started. Therefore, the external environment temperature did not change much, and its T_{ss} value is maintained at about 30°C. Since there is no constant temperature control, the external heat dissipation conditions of the battery are better.
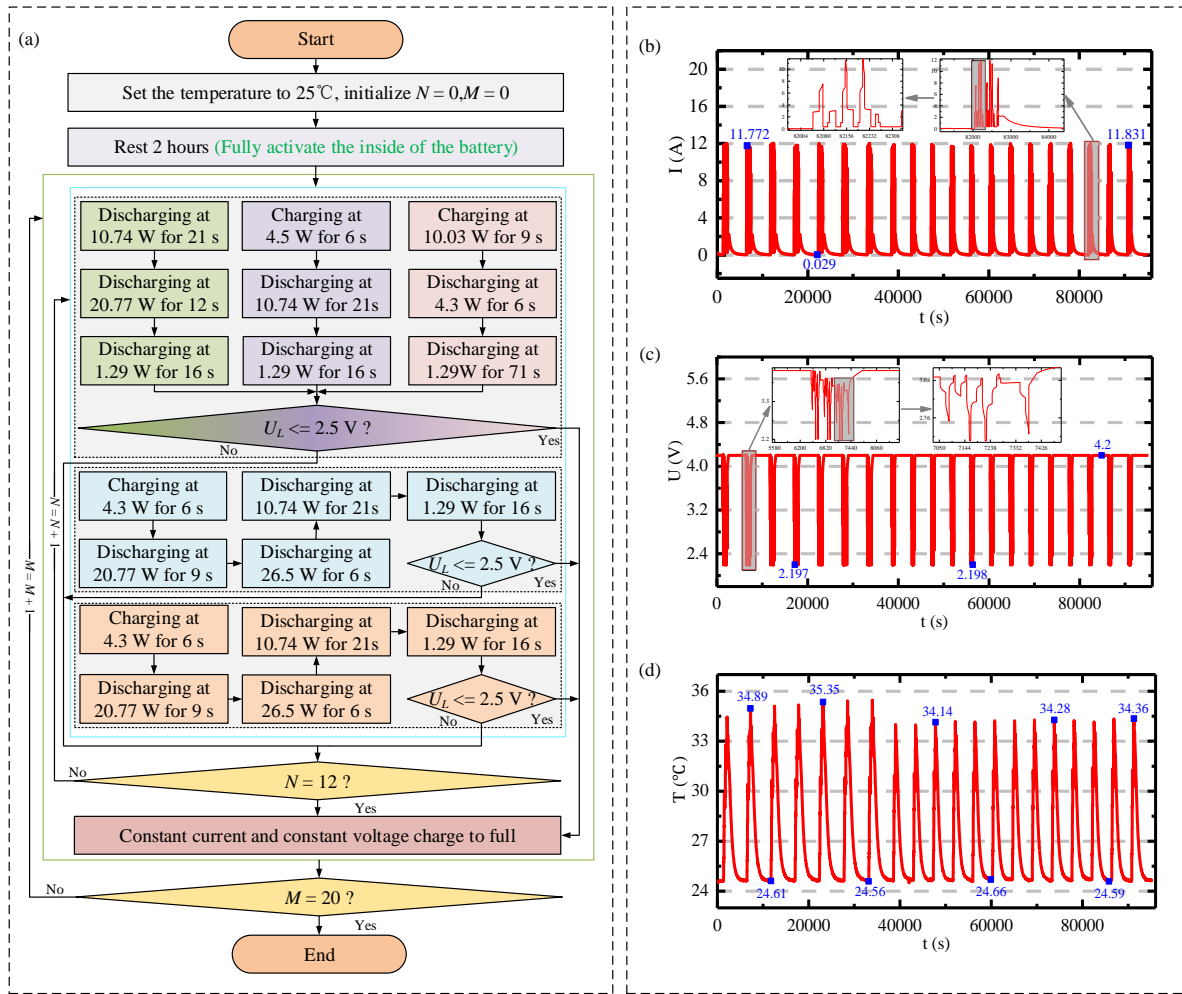
Fig. 5 BBDSTC experimental process and experimental results

3.2.3. FCFDT experiment at constant 45℃

To explore the adaptability of the model under constant high temperature, FCFDT experiment at constant 45℃ is further designed. Before the experiment, put the battery in a thermostat with a temperature of 45°C and let it stand for 1 hour to make the battery's own temperature and the ambient temperature balance. Then use a current pulse of 0.5 C to charge the battery with constant current and constant voltage to full, and then let it stand for 1 hour to balance the internal state of the battery. Then use 0.3 C, 1 C and 2 C current pulses to discharge the battery at a constant current to a cut-off voltage of 2.5 V. After each complete discharge, a 0.5 C current pulse is used to charge the battery with constant current and constant voltage to full. The whole experiment is carried out in a 45°C thermostat. The

FCFDT experiment process and experiment results are shown in Fig. (6). Among them, Fig. 6 (a) is the flow chart of the FCFDT experiment. Fig. 6(b) shows the current curve of the FCFDT experiment. Fig. 6(c) shows the terminal voltage curve of the FCFDT experiment. Fig. 6(d) shows the internal temperature curves of the FCFDT experiment.
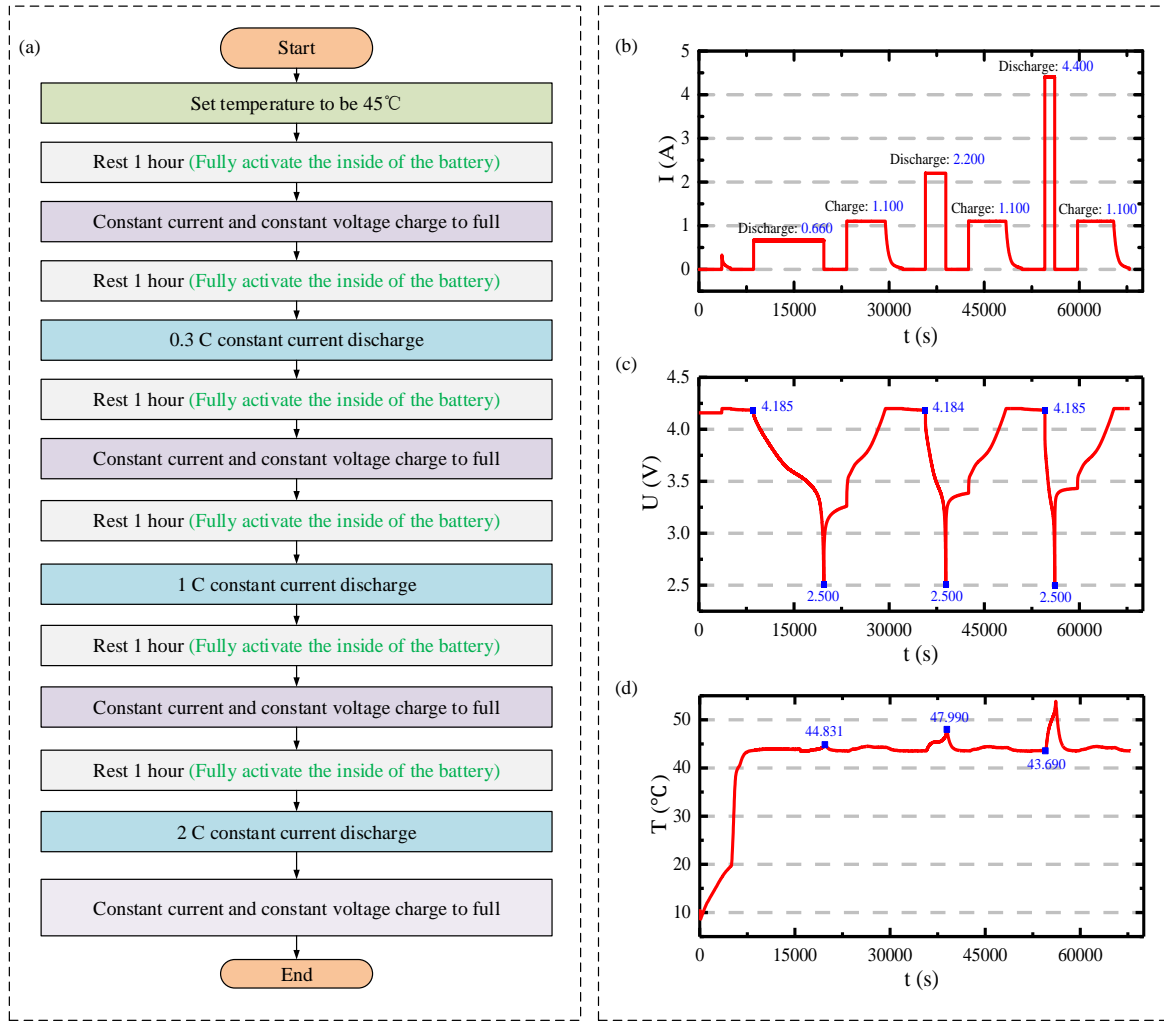

Fig. 6 FCFDT experimental process and experimental results

3.3. Model parameter identification and accuracy verification

The calculation of the battery heat source is central to the solution and verification of the entire thermal circuit system. The battery reaction heat Q_r is generated during the charge and discharge of the battery and is characterized in the model by the entropy heat coefficient dE/dT. The calculation of battery

heating power is the core of the solution and verification of the entire thermal circuit system. The battery reaction heat Q_r is generated during the charging and discharging of the battery, and is characterized by the entropy thermal coefficient dE/dT in the model. According to experiments, the dE/dT of the battery samples selected in this article is about 10^{-6} at different SOC values. Therefore, this paper ignores the Q_r term of the Bernardi equation when calculating the heating power of the battery, and uses the average value of the DC internal resistance of the battery sample to directly calculate the heating power of the battery. According to the core of the FFRLS algorithm shown in Fig. 2, combined with the HPPCC experimental data at a constant temperature of 25°C, the identification of C_i, R_i and C_s in the thermal circuit model of the selected battery sample is completed. The identification results of C_i, R_i and C_s are shown in Table 1.

Table 1 Identification results of C_i, R_i and C_s

LTCM Parameters	C_i (J/K)	C_s (J/K)	R_i (K/W)
Identification results	138.62	0.59	1.78

It should be noted that the thermal characteristic parameters C_i, R_i, and C_s in LTCM are deterministic, and their values will not change as the system application environment changes. However, the iterative calculation method of the FFRLS algorithm will lead to the existence of acceptable system noise in the identification results, which will further cause the thermal characteristic parameter results to produce changes within a small error range. Therefore, the identification results of C_i, R_i, and C_s in Table 2 are the time average of the iteration results of each parameter. In addition, by using the average value of the DC internal resistance of the battery sample to calculate the heating power of the battery, the calculation complexity of the model is reduced, and the application possibilities of the LTCM embedded system are improved. Using the identification results in Table 1, based on the experimental data under HPPCC experiment at constant 25°C, BBDST experiment at normal temperature and FCFDT
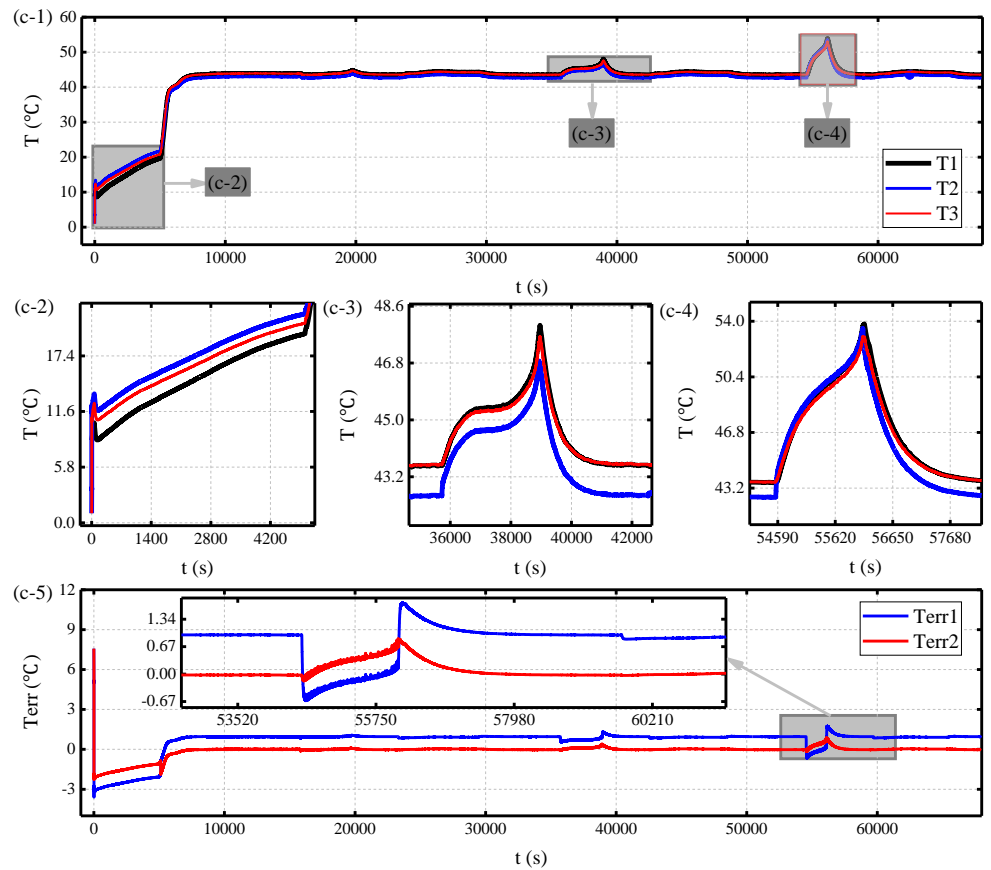
experiment at constant 45℃ respectively, the internal temperature of the battery is estimated under the

AFFRLS-JKF estimation strategy. Furthermore, this paper compares the prediction results under the

AFFRLS-JKF estimation strategy with the prediction results under the forgetting factor recursive least

squares - extended Kalman filter (FFRLS-EKF) estimation strategy to further verify the accuracy of

thermal characteristics modeling. The internal temperature prediction results for AFFRLS-JKF and

FFRLS-EKF estimation strategy under different working conditions are shown in Fig. 7.
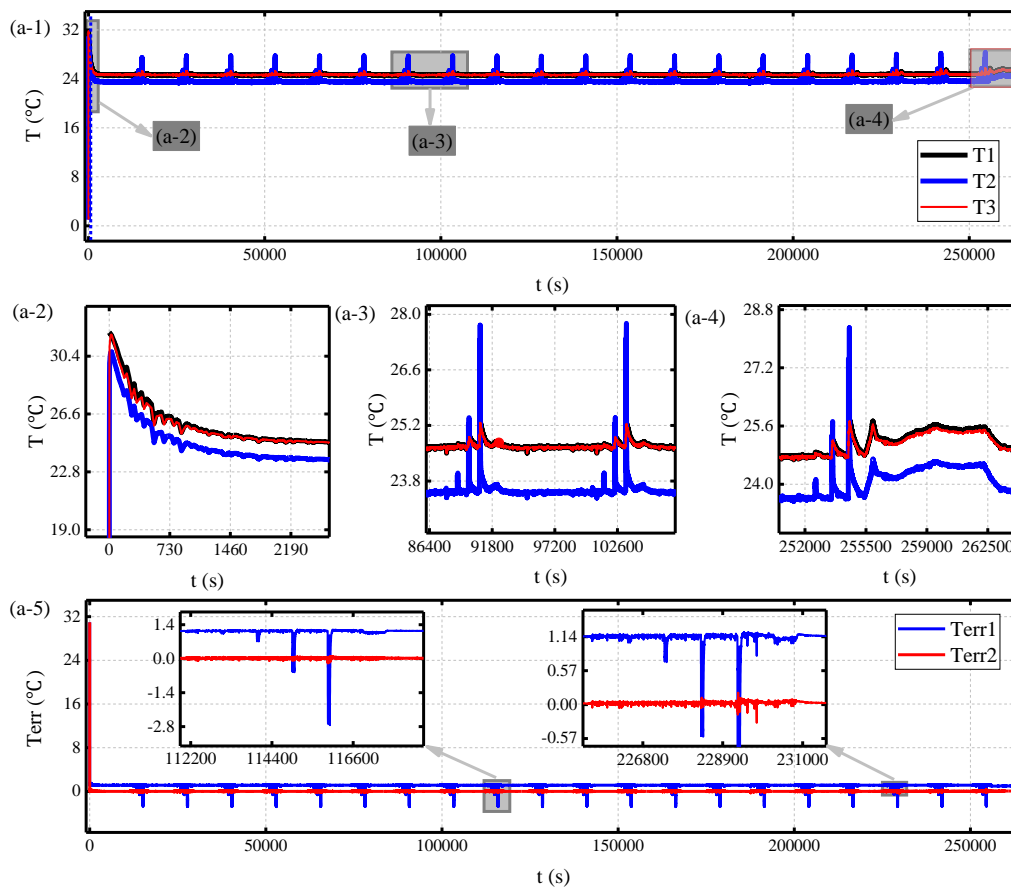
(a) T_{is} estimation results under CCDCT at constant 25°C
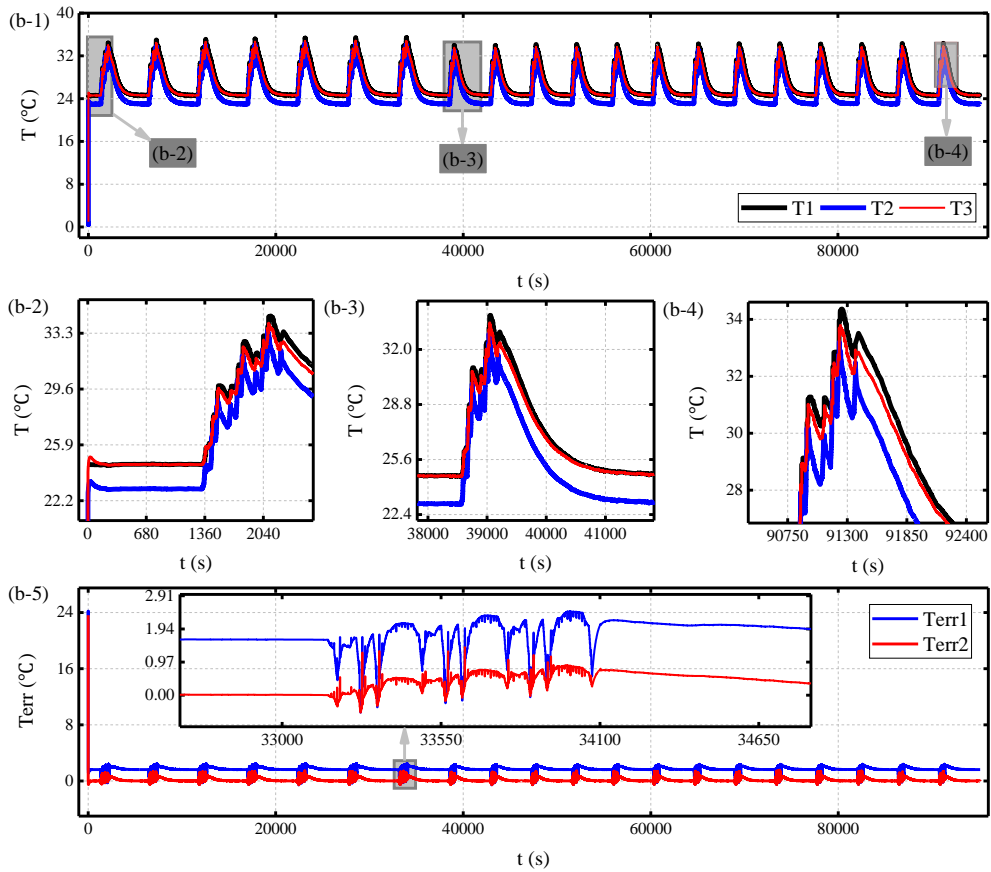
(b) T_{is} estimation results under BBDSTC at room temperature

(c) T_{is} estimation results under FCFDT at constant 45°C

Fig. 7 Estimation effect of T_{is} for AFFRLS-JKF and FFRLS-EKF under different working conditions

In Fig. 7, Fig. 7(a-1), Fig. 7(b-1) and Fig. 7(c-1) respectively represent the HPPCC experiment,

BBDSTC experiment and FCFDT experiment under the Tis estimation effect comparison curve. Among

them, T1 represents the measured value of T_{is} under different experimental conditions, and T2 represents

the estimated value of T_{is} for FFRLS-EKF estimation strategy under different experimental conditions,

and T3 represents the estimated value of T_{is} for AFFRLS-JKF estimation strategy under different

experimental conditions. Fig. 7(a-5), Fig. 7(b-5) and Fig. 7(c-5) respectively show the estimated error

curves of T_{is} under different working conditions. Among them, Terr1 represents the estimated error of

T_{is} for FFRLS-EKF estimation strategy under different working conditions, and Terr2 represents the

estimated error of T_{is} for AFFRLS-JKF estimation strategy under different working conditions. Fig.7(a-

2~4), Fig.7(b-2~4) and Fig.7(c-2~4) are the partial magnified curves under each working condition.

From Fig. 7 (a-5), (b-5) and (c-5), it can be seen that the estimation accuracy of the AFFRLS-JKF

estimation strategy is higher than that of the FFRLS-EKF under different working conditions. It proves

that the lumped thermal characteristics modeling method has high feasibility and accuracy.

To visually show the prediction precision for the AFFRLS-JKF estimation strategy under different

working conditions, the RMSE, MAPE, and MAXE indicators are used to quantitatively analyze the

estimated results after the algorithm is stabilized. In addition, when calculating the RMSE, MAPE, and

MAXE under AFFRLS-JKF and FFRLS-EKF, the experimental data after stabilization of the algorithm

are used to avoid systematic errors and measurement errors from interfering with the validation and

analysis of the model. Based on the calculation method of Equation (32), the calculation results of the

above quantitative indicators are obtained, as shown in Table 2.

It can be seen from Table 2 that the RMSE of the AFFRLS-JKF estimation strategy under the

HPPCC experiment, the BBDSTC experiment and the FCFDT experiment is lower than the FFRLS-

EKF estimation strategy by 0.31℃, 1.86℃ and 0.92℃, respectively. Compared with the FFRLS-EKF

estimation strategy, the MAPE of the AFFRLS-JKF estimation strategy under different conditions is reduced by 6.42%, 9.60% and 3.97%, respectively. The MAXE of the AFFRLS-JKF estimation strategy under different conditions is lower than that of the FFRLS-EKF estimation strategy by 2.34℃, 0.94℃ and 0.98℃, respectively. In addition, under HPPCC and BBDSTC conditions, the maximum internal temperature error based on the AFFRLS-JKF method is reduced by 1.36 °C and 0.27 °C, respectively, compared with the literature [9] (the maximum internal temperature estimated temperature difference under the low-temperature electro-thermal coupled model is 1.79 °C). The above quantitative calculation results fully verify the high-accuracy of the lumped thermal characteristics modeling method and the high-precision of the AFFRLS-JKF estimation strategy.

Table 2 Calculation results of RMSE, MAPE and MAXE for AFFRLS-JKF and FFRLS-EKF

| Estimation strategy	FFRLS-EKF			AFFRLS-JKF		
Evaluation index	RMSE (℃)	MAPE (%)	MAXE (℃)	RMSE (℃)	MAPE (%)	MAXE (℃)
HPPCC at constant 25°C	1.36	6.55	2.77	0.05	0.13	0.43
BBDSTC at room temperature	2.27	10.76	2.46	0.41	1.16	1.52
FCFDT at constant 45°C	1.45	5.37	3.17	0.53	1.40	2.19

3.4. Robustness analysis of external thermal resistance identification

The complex and variable usage environment of the battery leads to the external thermal resistance R_o in LTCM cannot be identified in advance. Therefore, the accuracy verification of the model and the precision verification study of the algorithm need to consider the convergence and stability of the external thermal resistance R_o. When using the AFFRLS-JKF algorithm for online adaptive identification and estimation of the thermal path model of the battery, the initialization of R_o often has large deviations.

In order to further verify the adaptive capability of LTCM to the external environment, the robustness of the model to the initial values under different operating conditions and different external environments needs to be analyzed. In this paper, based on the HPPCC experiment at 25°C, the BBDST experiment at room temperature and the FCFDT experiment at 45°C, the external thermal resistance R_o in LTCM is initialized to 0.01 °C/W, 5 °C/W, 15 °C/W, 25 °C/W and 35 °C/W, respectively, to investigate the convergence and stability of the external thermal resistance R_o estimation results. The estimation results of the external thermal resistance R_o at different initial values and under different operating conditions are shown in Fig. 8.
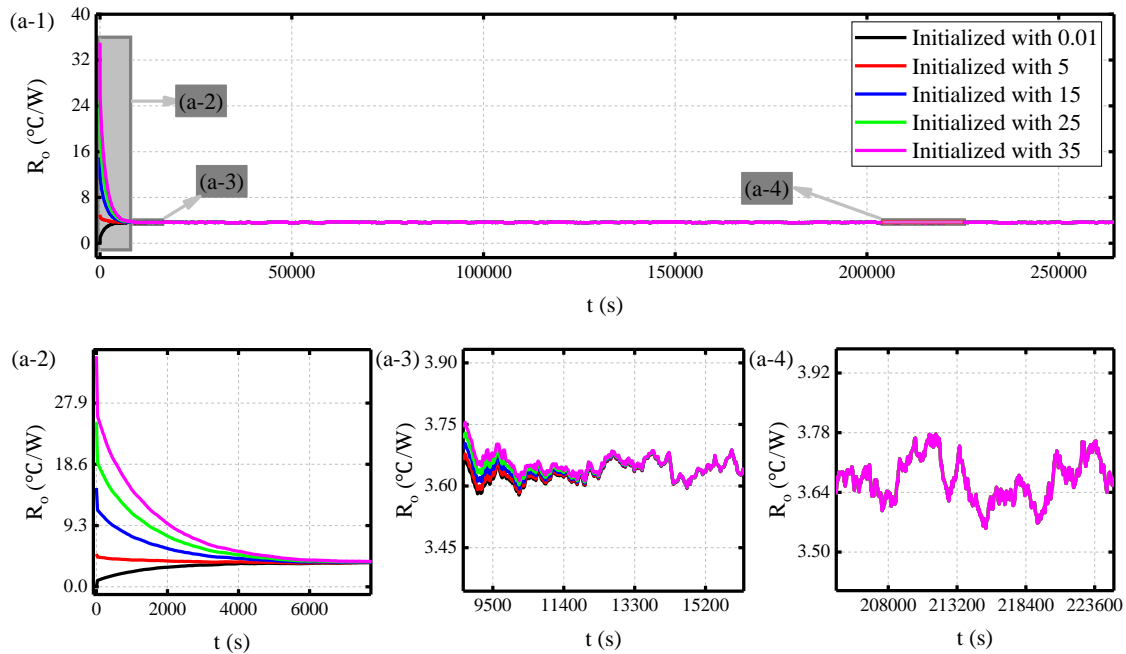
(a) Change rule of R_o under constant 25°C CCDCT experiment
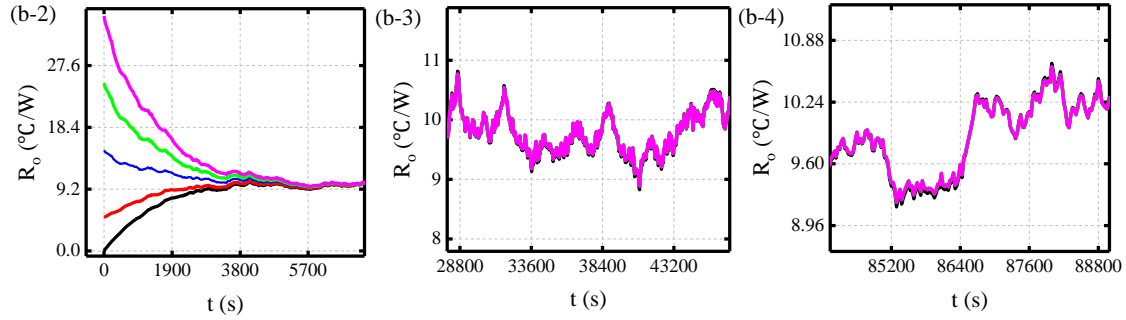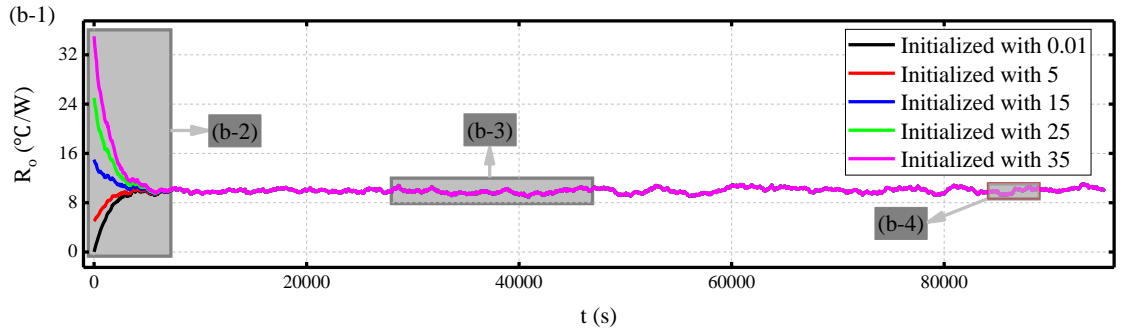
(b) Change rule of R_o under room temperature BBDSTC experiment
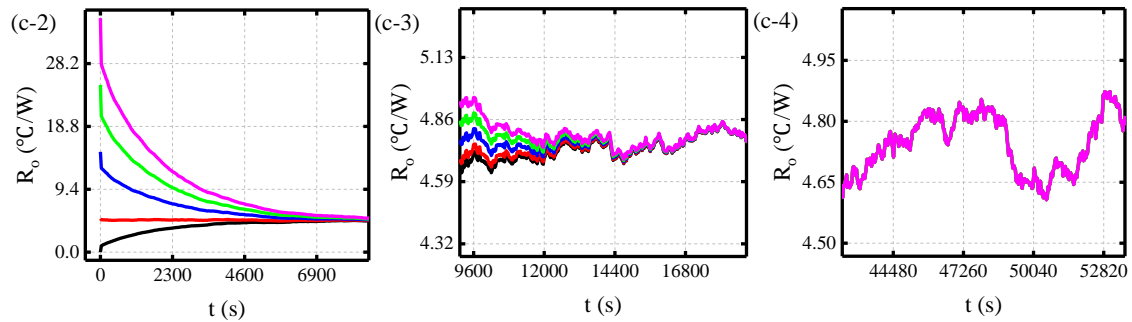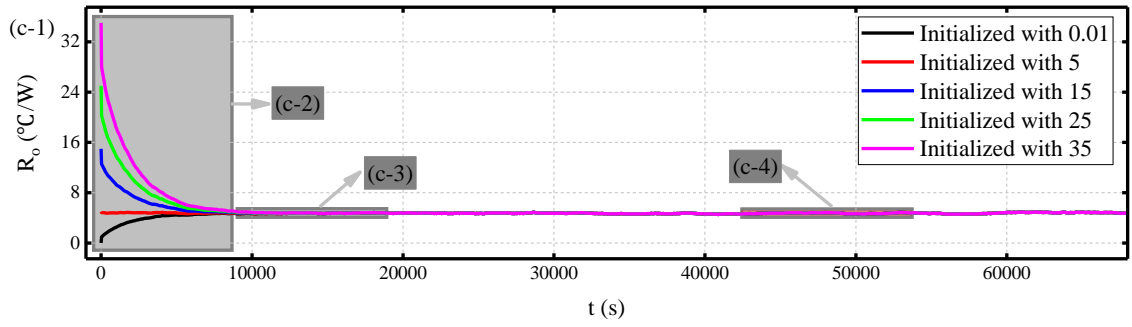
(c) Change rule of R_o under constant 45°C FCFDT experiment

Fig.8 Effect of different initial values on R_o under different complex working conditions

Fig. 8(a-1), Fig. 8(b-1) and Fig. 8(c-1) show the curves of the estimated external thermal resistance R_o under the HPPCC experiment, BBDSTC experiment and FCFDT experiment, respectively. Fig. 8(a-2~4), Fig. 8(b-2~4) and Fig. 8(c-2~4) show the local magnification curves at special locations. The

experimental results under different operating conditions show that the LTCM has a strong adaptive adjustment capability to the R_o initialization error. With the increase of the system data input and the number of iterations of AFFRLS-JKF algorithm, the value of external thermal resistance R_o stabilizes indicating that LTCM has strong stability. The convergence times and stability values for the HPPCC experiment at constant 25°C, the BBDST experiment at room temperature, and the FCFDT experiment at constant 45°C are given in Table 3. It can be seen from Table 3 that the convergence time of R_o under the HPPCC experiment, BBDSTC experiment and FCFDT experiment are 7856 s, 4657 s and 9862 s, respectively, and the convergence values are 3.652 ℃/W, 10.147 ℃/W and 4.765 ℃/W, respectively. In addition, it can be seen that different external environmental conditions will lead to different convergence times and convergence values, but they will eventually converge to the same value. It is fully verified that the LTCM model has strong adaptability to the complex operating conditions of the battery.

Table 3 Convergence time and convergence value of R_o under different working conditions

Evaluation indicators	HPPCC at constant 25°C	BBDSTC at room temperature	FCFDT at constant 45°C
Convergence time (s)	7853	4657	9862
Convergence value (℃/W)	3.652	10.147	4.765

4. Conclusion

The high-accuracy estimation of the internal temperature of lithium-ion battery is the key to the safe and reliable operation of BMS. This paper solves the problem of online high-precision adaptive estimation of the battery internal temperature by establishing the LTCM based on circuit theory. By analyzing the mechanism of heat generation and heat dissipation inside the battery, the discrete state-space equation expression of the thermal characteristic model is realized by combining the control theory.

Considering the uncertainty of external thermal resistance, the AFFRLS-JKF algorithm is proposed to realize the co-estimation of the parameters of the LTCM and the internal temperature of the battery. In addition, in order to verify the accuracy of the battery thermal characteristics modeling and the precision of the AFFRLS-JKF estimation strategy, the HPPCC experiment at 25℃, the BBDST experiment at room temperature and the FCFDT experiment at 45℃ designed and completed respectively. The experimental results show that AFFRLS-JKF has significantly lower RMSE, MAPE and MAXE calculation results than RRLRS-EKF, which verifies the high accuracy of the AFFRLS-JKF strategy and the high accuracy of lumped heat modeling. In addition, the robustness of LTCM to the initial value under different working conditions and different external environments is analyzed. The results show that the convergence time of R_o under different conditions is 7856 s, 4657 s and 9862 s respectively, which further verifies that the LTCM based on the AFFRLS-JKF estimation strategy has strong robustness. The lumped thermal characteristic modeling method can provide theoretical and experimental basis for the real-time estimation of the internal temperature of the lithium-ion battery and the safe thermal management of the battery.

Acknowledgments

References

[1] Raijmakers, L.H.J.; Danilov, D.L.; Eichel, R.A.; Notten, P.H.L. A review on various temperature-indication methods for Li-ion batteries. *Applied Energy* **2019**, *240*, 918-945.

[2] Hueso, K.B.; Armand, M.; Rojo, T. High temperature sodium batteries: status, challenges and future trends. *Energy & Environmental Science* **2013**, *6*, 734-749.

[3] Yu, X.; Sandhu, N.S.; Yang, Z.Y.; Zheng, M. Suitability of energy sources for automotive application - A review. *Applied Energy* **2020**, *271*, 115169, 1-16.

[4] Hu, X.S.; Li, S.B.; Peng, H.; Sun, F.C. Charging time and loss optimization for LiNMC and LiFePO$_4$ batteries based on equivalent circuit models. *Journal of Power Sources* **2013**, *239*, 449-457.

[5] Feng, X.N.; Pan, Y.; He, X.M.; Wang, L.; Ouyang, M.G. Detecting the internal short circuit in large-format lithium-ion battery using model-based fault-diagnosis algorithm. *Journal of Energy Storage* **2018**, *18*, 26-39.

[6] Tao, F.B.; Zhang, W.J.; Guo, D.L.; Cao, W.J.; Sun, L.; Jiang, F.M. Thermofluidic modeling and temperature monitoring of Li-ion battery energy storage system. *Applied Thermal Engineering* **2020**, *181*, 116026, 1-13.

[7] Li, Y.Y.; Stroe, D.I.; Cheng, Y.H.; Sheng, H.M.; Sui, X.; Teodorescu, R. On the feature selection for battery state of health estimation based on charging-discharging profiles. *Journal of Energy Storage* **2021**, *33*, 102122, 1-16.

[8] Jaguemont, J.; Boulon, L.; Dube, Y. A comprehensive review of lithium-ion batteries used in hybrid and electric vehicles at cold temperatures. *Applied Energy* **2016**, 1*64*, 99-114.

[9] Jiang, J.C.; Ruan, H.J.; Sun, B.X.; Zhang, W.G.; Gao, W.Z.; Wang, L.Y.; Zhang, L.J. A reduced low-temperature electro-thermal coupled model for lithium-ion batteries. *Applied Energy* **2016**, *177*, 804-816.

[10] Oh, Y.S.; Kim, J.H.; Xie, Z.Q.; Cho, S.J.; Han, H.; Jeon, S.W.; Park, M.; et al. Battery-free, wireless soft sensors for continuous multi-site measurements of pressure and temperature from patients at risk for pressure injuries. *Nature Communications* **2021**, *12*, 5008, 1-16.

[11] Chen, J.; Ren, D.S.; Hsu, H.J.; Wang, L.; He, X.M.; Zhang, C.P.; Feng, X.N.; Ouyang, M.G. Investigating the thermal runaway features of lithium-ion batteries using a thermal resistance network model. *Applied Energy* **2021**, *295*, 117038, 1-13.

[12] Mao, B.B.; Liu, C.Q.; Yang, K.; Li, S.; Liu, P.J.; Zhang, M.J.; Meng, X.D.; Gao, F.; Duan, Q.L.; Wang, Q.S. Thermal runaway and fire behaviors of a 300 Ah lithium ion battery with LiFePO$_4$ as cathode. *Renewable & Sustainable Energy Reviews* **2021**, 139, 110717, 1-14.

[13] Yu, Y.F.; Vergori, E.; Worwood, D.; Tripathy, Y.; Guo, Y.; Soma, A.; Greenwood, D.; Marco, J. Distributed thermal monitoring of lithium-ion batteries with optical fibre sensors. *Journal of Energy Storage* **2021**, 39, 102560, 1-11.

[14] Wang, H.B.; Chen, S.Q.; Du, Z.M. Side plate-based cell-to-pack LiNi$_{0.5}$Co$_{0.2}$Mn$_{0.3}$O$_2$ lithium battery module design with internal temperature acquisition and precise thermal modeling. *International Journal of Energy Research* **2021**, 1-10.

[15] Karimi, D.; Behi, H.; Hosen, M.S.; Jaguemont, J.; Berecibar, M.; Van Mierlo, J. A compact and optimized liquid-cooled thermal management system for high power lithium-ion capacitors. *Applied Thermal Engineering* **2021**, 185, 116449, 1-14.

[16] Jeong, K.; Cho, H.H.; Han, H.N.; Dunand, D.C. A fully coupled diffusional-mechanical finite element modeling for tin oxide-coated copper anode system in lithium-ion batteries. *Computational Materials Science* **2020**, *172*, 109343, 1-10.

[17] Ohashi, A.; Kodama, M.; Sun X.Y.; Hori, S.; Suzuki, K.; Kanno, R.; Hirai, S. Stress distribution in the composite electrodes of sulfide all-solid-state lithium-ion batteries. *Journal of Power Sources* **2020**, *470, 228437*, 1-10.

[18] Tian, H.K.; Chakraborty, A.; Talin, A.A.; Eisenlohr, P.; Qi, Y. Evaluation of The Electrochemo-Mechanically Induced Stress in All-Solid-State Li-Ion Batteries. *Journal of The Electrochemical Society* **2020**, *167*, *090541*, 1-11.

[19] Xie, Y.; Li, W.; Hu, X.S.; Zou, C.F.; Feng, F.; Tang, X.L. Novel Mesoscale Electrothermal Modeling for Lithium-Ion Batteries. *IEEE Transactions on Power Electronics* **2020**, *35*, 2595-2614.

[20] Lee, D.; Koo, B.; Shin, C.B.; Lee, S.Y.; Song, J.; Jang, I.C.; Woo, J.J. Modeling the Effect of the Loss of Cyclable Lithium-on the Performance Degradation of a Lithium-Ion Battery. *Energies* **2019**, *12*, 4386, 1-14.

[21] Noh, T.W.; Ahn, J.H.; Lee, B.K. Cranking Capability Estimation Algorithm Based on Modeling and Online Update of Model Parameters for Li-Ion SLI Batteries. *Energies* **2019**, *12*, 3365, 1-14.

[22] Pajkossy, T.; Jurczakowski, R. Electrochemical impedance spectroscopy study of lithium-ion capacitors: Modeling and capacity fading mechanism. *Current Opinion in Electrochemistry* **2017**, *1*, 53-58.

[23] Droste, A.M.; Pape, J.J.; Overeem, A.; Leijnse, H.; Steeneveld, G.J.; Van Delden, A.J.; Uijlenhoet, R. Crowdsourcing Urban Air Temperatures through Smartphone Battery Temperatures in Sao Paulo, Brazil. *Journal of Atmospheric and Oceanic Technology* **2017**, *34*, 853-1866.

[24] Li, H.H.; Wang, X.Y.; Saini, A.; Zhu, Y.Q.; Wang, Y.P. State of Charge Estimation for Lithium-Ion Battery Models Based on a Thermoelectric Coupling Model. *International Journal of Electrochemical Science* **2020**, *15*, 3807-3824.

[25] Howey, D.A.; Yufit, V.; Offer, G.J.; Brandon, N.P. Online Measurement of Battery Impedance Using Motor Controller Excitation. *IEEE Transactions on Vehicular Technology* **2014**, *63*, 2557-2566.

[26] Koseoglou, M.; Tsioumas, E.; Ferentinou, D.; Jabbour, N.; Papagiannis, D.; Mademlis, C. Lithium plating detection using dynamic electrochemical impedance spectroscopy in lithium-ion batteries. *Journal of Power Sources* **2021**, *512*, 230508, 1-10.

[27] Gargh, P.; Sarkar, A.; Lui, Y. H.; Shen, S.; Hu, C.; Hu, S.; Nlebedim, I.C.; Shrotriya, P. Correlating capacity fade with film resistance loss in fast charging of lithium-ion battery. *Journal of Power Sources* **2021**, *485*, 229360, 1-7.

[28] Koseoglou, M.; Tsioumas, E.; Papagiannis, D.; Jabbour, N.; Mademlis, C. A Novel On-Board Electrochemical Impedance Spectroscopy System for Real-Time Battery Impedance Estimation. *IEEE Transactions on Power Electronics* **2021**, *36*, 10776-10787.

[29] Chen, X.; Li, L.Y.; Liu, M.M.; Huang, T.; Yu, AS. Detection of lithium plating in lithium-ion batteries by distribution of relaxation times. *Journal of Power Sources* **2021**, *496*, 229867, 1-9.

[30] Babaeiyazdi, I.; Rezaei-Zare, A.; Shokrzadeh, S. State of charge prediction of EV Li-ion batteries using EIS: A machine learning approach. *Energy* **2021**, *223*, 120116, 1-9.

[31] Liu, G.Z.; Yuan, X.G.; Yang, Y.M.; Tao, J.M.; Chi, Y.B.; Hong, L.Y.; Lin, Z.Y.; Lin, Y.B. Three-dimensional hierarchical wreath-like CO3O4@ TiO2 as an anode for lithium-ion batteries. *Journal of Alloys and Compounds* **2019**, *780*, 948-958.

[32] Xu, H.J.; Wang, J.X.; Li, Y.Z.; Bi, Y.J.; Gao, L. A Thermoelectric-Heat-Pump Employed Active Control Strategy for the Dynamic Cooling Ability Distribution of Liquid Cooling System for the Space Station's Main Power-Cell-Arrays. *Entropy* **2019**, *21*, 578, 1-24.

[33] Ran, X.X.; Tao, J.M.; Chen, Z.Y.; Yan, Z.R.; Yang, Y.M.; Li, J.X.; Lin, Y.B.; Huang, Z.G. Surface heterostructure induced by TiO2 modification in Li-rich cathode materials for enhanced electrochemical performances. *Electrochimica Acta* **2020**, *353*, 135959, 1-10.

[34] Wu, X.G.; L.V.; S.Y.; Chen, J.Z. Determination of the Optimum Heat Transfer Coefficient and Temperature Rise Analysis for a Lithium-Ion Battery under the Conditions of Harbin City Bus Driving Cycles. *Energies* **2017**, *10*, 1723, 1-17.

[35] Fleckenstein, M.; Fischer, S.; Bohlen, O. Thermal Impedance Spectroscopy - A method for the thermal characterization of high power battery cells. *Journal of Power Sources* **2013**, *223*, 259-267.

[36] Saw, L.H.; Poon, H.M.; Thiam, H.S.; Cai, Z.S.; Chong, W.T.; Pambudi, N.A.; King, Y.J. Novel thermal management system using mist cooling for lithium-ion battery packs. *Applied Energy* **2018**, *223*, 146-158.

[37] Liu, X.T.; Chen, Z.H.; Zhang, C.B.; Wu, J. A novel temperature-compensated model for power Li-ion batteries with dual-particle-filter state of charge estimation. *Applied Energy* **2014**, *123*, 263-272.

[38] Xu, X.H.; Li, W.Z.; W Xu, B.; Qin, J. Numerical study on a water cooling system for prismatic LiFePO4 batteries at abused operating conditions. *Applied Energy* **2019**, *250*, 404-412.

[39] Jiang, Z.Y.; Qu, Z. G. Lithium-ion battery thermal management using heat pipe and phase change material during discharge-charge cycle: A comprehensive numerical study. *Applied Energy* **2019**, *242*, 378-392.

[40] Ling, Z.Y.; Lin, W.Z.; Zhang, Z.G.; Fang, X.M. Computationally efficient thermal network model and its application in optimization of battery thermal management system with phase change materials and long-term performance assessment, *Applied Energy* **2020**, *259*, 114120, 1-9.

[41] Chen, Z.Y.; Zhang, B.; Xiong, R.; Shen, W.X.; Yu, Q.Q. Electro-thermal coupling model of lithium-ion batteries under external short circuit, *Applied Energy* **2021**, *293*, 116910, 1-13.

[42] Shi, HT; Wang, SL; Wang, LP; Xu, WH; Carlos, F; Dablu, BE; Zhang,YC. On-line adaptive asynchronous parameter identification of lumped electrical characteristic model for vehicle lithium-ion battery considering multi-time scale effects. *Journal of Power Sources* **2022**; *515*: 230725.